

Supporting Information

Fast-Charging Batteries based on Dual-Halogen Solid-State Electrolytes

Hongtu Zhang,^{#a} Xiaomeng Shi,^{#a} Zhichao Zeng,^{*a} Yabin Zhang,^b Yaping Du^{*ac}

^a Tianjin Key Lab for Rare Earth Materials and Applications, Center for Rare Earth and Inorganic Functional Materials, Smart Sensing Interdisciplinary Science Center, School of Materials Science and Engineering, National Institute for Advanced Materials, Nankai University, Tongyan Road No.38, Tianjin 300350, China

^b State Key Laboratory of Featured Metal Materials and Life-cycle Safety for Composite Structures, MOE Key Laboratory of New Processing Technology for Nonferrous Metals and Materials, and School of Resources, Environment and Materials, Guangxi University, Nanning 530004, China

^c Haihe Laboratory of Sustainable Chemical Transformations, Tianjin 300192, China

[#] These two authors contributed equally to this work.

Table of Contents

Experiment Section

Materials Characterizations

Electrochemical Measurements

Bond Valence Site Energy (BVSE) Calculations

Fig. S1. SEM and EDS results for $\text{Li}_3\text{YCl}_5\text{I}_1$.

Fig. S2. The Arrhenius conductivity plots of $\text{Li}_3\text{YCl}_{6-x}\text{I}_x$.

Fig. S3. The activation energy of $\text{Li}_3\text{YCl}_{6-x}\text{I}_x$.

Fig. S4. Direct current polarization curve of $\text{Li}_3\text{YCl}_5\text{I}_1$.

Fig. S5. Li^+ ion migration pathways in $\text{Li}_3\text{YCl}_5\text{I}_1$.

Fig. S6. BVSE models of two migration pathways in $\text{Li}_3\text{YCl}_5\text{I}_1$.

Fig. S7. FWHM and chemical shifts of the temperature-dependent NMR peaks of $\text{Li}_3\text{YCl}_5\text{I}_1$.

Fig. S8. GITT result for $\text{Li}_4\text{Ti}_5\text{O}_{12}$.

Fig. S9. Performance of $\text{Li-Li}_4\text{Ti}_5\text{O}_{12}$ cells at 1.0 C.

Fig. S10. Cross-section SEM and EDS images of $\text{Li-Li}_4\text{Ti}_5\text{O}_{12}$ cell.

Figure S11. Performances of $\text{Li-Li}_4\text{Ti}_5\text{O}_{12}$ cells at 0.1 C and 1.0 C.

Table S1-S2. Atomic coordinates of Li_3YCl_6 and $\text{Li}_3\text{YCl}_5\text{I}_1$ obtained from XRD Rietveld refinement.

Table S3. Lattice parameters of Li_3YCl_6 and $\text{Li}_3\text{YCl}_5\text{I}_1$ obtained from XRD Rietveld refinement.

Table S4. Bond lengths of Li-Cl in Li_3YCl_6 and $\text{Li}_3\text{YCl}_5\text{I}_1$.

References

Experimental Section

Synthesis of $\text{Li}_3\text{YCl}_{6-x}\text{I}_x$

Stoichiometric LiCl (Macklin, 99%), LiI (Macklin, 99%) and YCl_3 (Aladdin, 99.95%) powders were mixed and then hand-ground for 15 min. The mixture was pressed into a thin pellet at a pressure of 4 tons. The pellet was then transferred to a crucible and annealed for 12 h. The annealing temperature was 450 °C, and the heating and cooling rates were both 2 °C/min. After the annealing process, the pellet was ground to a powder for the following characterizations. The above procedures were all carried out in a glove box filled with argon.

Materials Characterizations

X-ray diffraction (XRD) was performed on a Rigaku Miniflex600 diffractometer and a Rigaku Smart Lab 3kW diffractometer with scan rates of 3° min⁻¹ and 1° min⁻¹, respectively. Cu K α radiation was used in both instruments with a step size of 0.01°. The XRD data was collected in an argon-atmosphere. XRD Rietveld refinement was performed with GSAS-EXPGUI, and the crystal structures were mapped with the help of VESTA.^[1, 2]

⁷Li Magic angle spinning nuclear magnetic resonance (MAS-NMR) was performed on a Bruker Avance III WB 400 (9.4 T). A 4 mm commercial probe was equipped and applied. 0 ppm in the ⁷Li NMR spectrum was calibrated with 1 M LiCl aqueous solution. The Ramohr frequency is 155.53 MHz.

Scanning electron microscopy (SEM) and energy dispersive spectroscopy (EDS) were used to observe the morphologies and elemental distributions of the samples. The test samples were prepared in an argon-atmosphere.

Thermo Scientific ESCALAB 250Xi was used to perform X-ray photoelectron spectroscopy (XPS).

Electrochemical Measurements

Electrochemical impedance spectroscopy (EIS) was performed on an Autolab PGSTAT302N instrument with a frequency range from 10⁶ Hz to 1 Hz at room-temperature. Approximately 80 mg of electrolyte was cold pressed into a pellet (diameter: 10 mm) under 4 tons, and a thin layer of Ketjen Black (ECP 200 L) was used as the blocking electrode for the EIS measurement.

Cycling voltammetry (CV) was carried out on CHI660E at room temperature. For the Li/Li₇P₃S₁₁ (HF-Kejing, 99.99%)/Li₃YCl₅I₁/Li₃YCl₅I₁-C cell test, the scan rate was 0.1 mV/s in a potential range of -0.5 V ~ 5 V versus Li⁺/Li, and the mass ratio of Li₃YCl₅I₁ to the carbon used in the cathode was 9 : 1. For the test of the Li-In/Li₇P₃S₁₁/Li₃YCl₅I₁/Li₄Ti₅O₁₂-Li₃YCl₅I₁-C cell, the scan rate was 0.1 mV/s in a potential range of 1.2 V ~ 2.4 V versus Li⁺/Li, and the

mass ratio of $\text{Li}_4\text{Ti}_5\text{O}_{12}$ (3A, 99.9%), $\text{Li}_3\text{YCl}_5\text{I}_1$ and carbon used in the cathode was 19 : 80 : 1. Ketjen Black (ECP 200 L) was used as the aforementioned carbon, and pretreatment at 600 °C for 3 h in an argon-atmosphere was performed.

The Galvanostatic intermittent titration technique (GITT) was carried out on a LANHE CT2001A. The batteries were fabricated as $\text{Li-In/Li}_7\text{P}_3\text{S}_{11}/\text{Li}_3\text{YCl}_5\text{I}_1/\text{Li}_4\text{Ti}_5\text{O}_{12}-\text{Li}_3\text{YCl}_5\text{I}_1-\text{C}$ for the GITT test. The cyclic rate was 0.05 C, the pulse time was 5 min, and the relaxation time was 10 min.

The Li-In symmetric cells with configurations of $\text{Li-In/Li}_3\text{YCl}_5\text{I}_1/\text{Li-In}$ and $\text{Li-In/Li}_7\text{P}_3\text{S}_{11}/\text{Li}_3\text{YCl}_5\text{I}_1/\text{Li}_7\text{P}_3\text{S}_{11}/\text{Li-In}$ were cold pressed. In the symmetric cells, 80 mg $\text{Li}_3\text{YCl}_5\text{I}_1$ was used, and the weight of $\text{Li}_7\text{P}_3\text{S}_{11}$ on one side was approximately 8 mg. The Li-In symmetric cells were tested on a LANHE CT2001A, and the current density was 0.1 mA cm⁻². The Li- $\text{Li}_4\text{Ti}_5\text{O}_{12}$ cells were fabricated as $\text{Li-In/Li}_7\text{P}_3\text{S}_{11}/\text{Li}_3\text{YCl}_5\text{I}_1/\text{Li}_4\text{Ti}_5\text{O}_{12}-\text{Li}_3\text{YCl}_5\text{I}_1-\text{C}$. The weight of $\text{Li}_7\text{P}_3\text{S}_{11}$ was approximately 8 mg. The weight ratio of the cathodal components was $\text{Li}_4\text{Ti}_5\text{O}_{12} : \text{Li}_3\text{YCl}_5\text{I}_1 : \text{C} = 19 : 80 : 1$, and the whole cathode was weighed as 7 mg. 80 mg of $\text{Li}_3\text{YCl}_5\text{I}_1$, $\text{Li}_7\text{P}_3\text{S}_{11}$, Li-In alloy and the cathode were cold pressed into a pellet (diameter : 10 mm) at a pressure of 4 tons in an argon-filled glovebox, and then sealed in a 2032-type coin cell. The Li- $\text{Li}_4\text{Ti}_5\text{O}_{12}$ cells were tested on a LANHE CT2001A in a voltage range of 1.2 V ~ 2.4 V versus Li^+/Li .

Bond Valence Site Energy (BVSE) Calculations

BVSE calculations are performed by the softBV software to study the Li^+ ion migration pathways.^[3] The resolution of the grid of the points was 0.1 Å. The BVSE maps show the preferred Li^+ ion migration pathways.

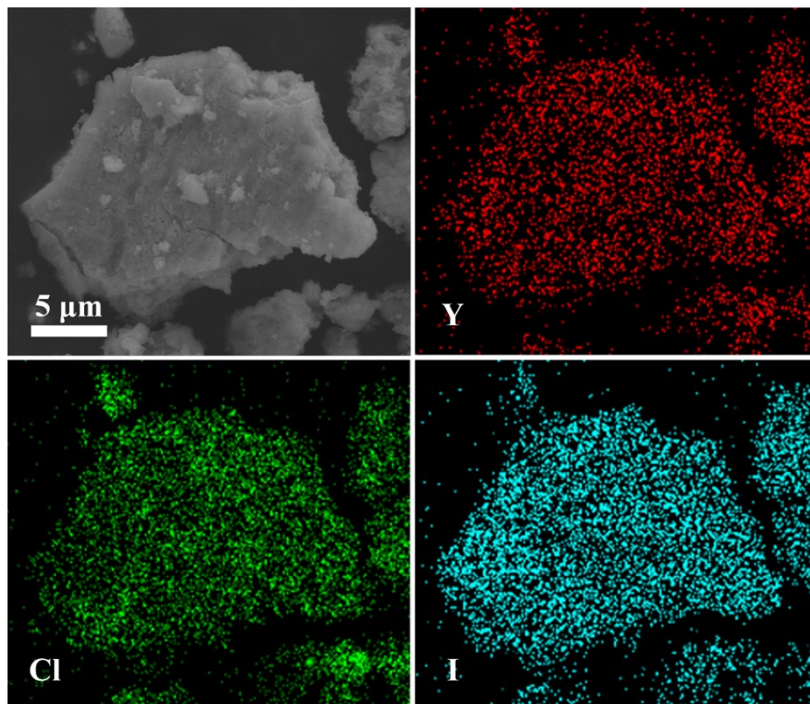


Figure S1. The SEM image and EDS elemental mapping of $\text{Li}_3\text{YCl}_5\text{I}_1$ show a uniform elemental distribution.

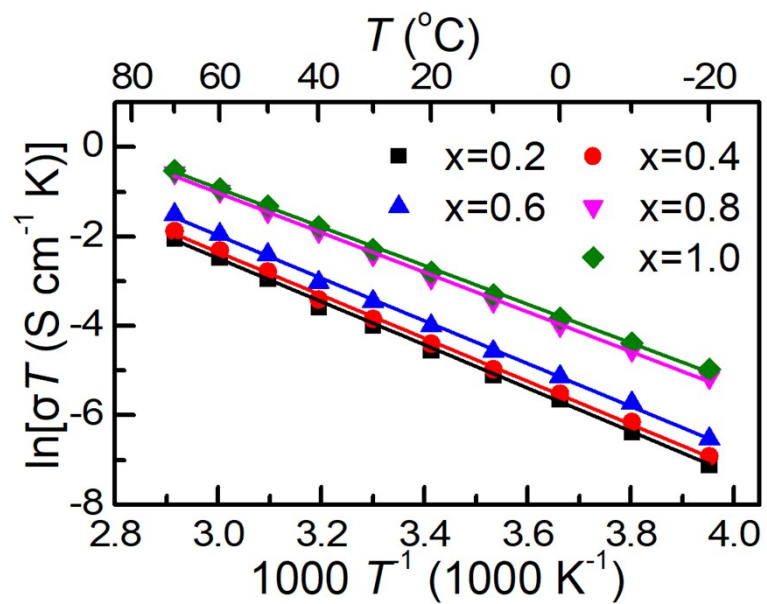


Figure S2. The Arrhenius conductivity plots of $\text{Li}_3\text{YCl}_{6-x}\text{I}_x$.

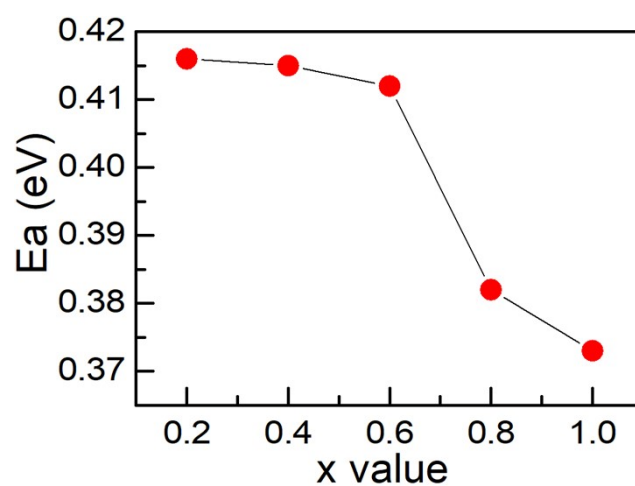


Figure S3. The activation energy of $\text{Li}_3\text{YCl}_{6-x}\text{I}_x$.

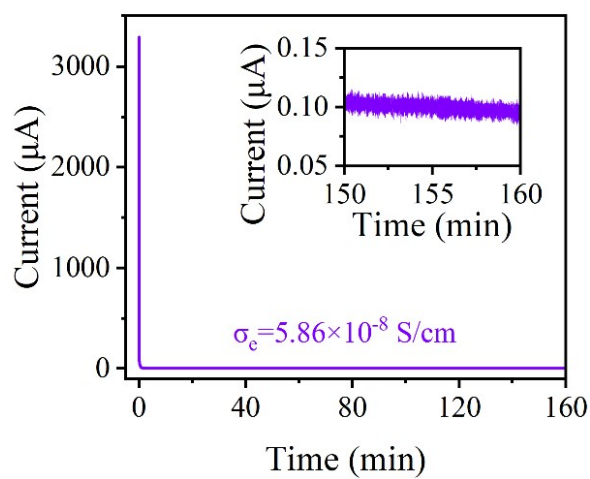


Figure S4. The direct current polarization curve of $\text{Li}_3\text{YCl}_5\text{I}_1$.

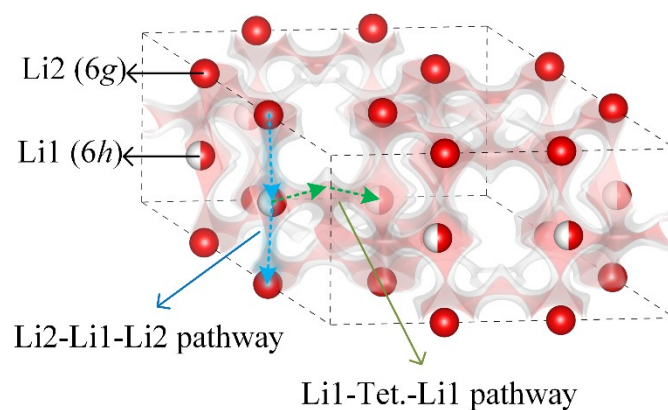


Figure S5. The Li^+ ions migration pathways in $\text{Li}_3\text{YCl}_5\text{I}_1$. The red isosurface denotes the Li^+ probability density.

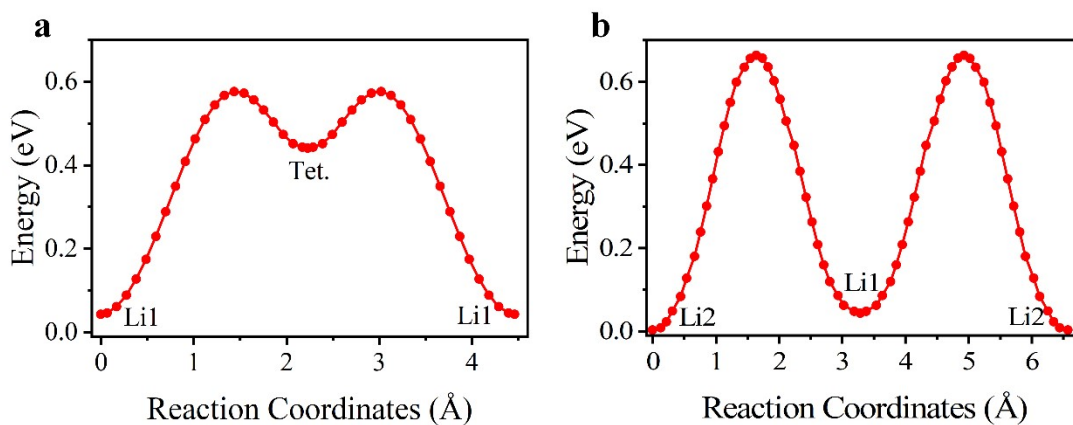


Figure S6. (a) The BVSE model of [Li1-Tet.-Li1] pathway in $\text{Li}_3\text{YCl}_5\text{I}_1$; (b) The BVSE model of [Li2-Li1-Li2] pathway in $\text{Li}_3\text{YCl}_5\text{I}_1$.

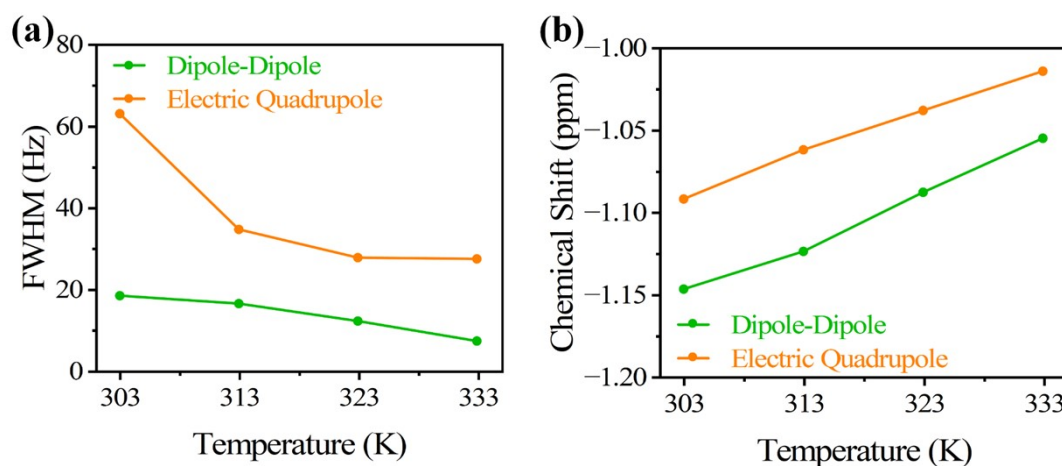


Figure S7. The change in (a) FWHM and (b) chemical shifts of the temperature-dependent NMR peaks of ^7Li in $\text{Li}_3\text{YCl}_5\text{I}_1$.

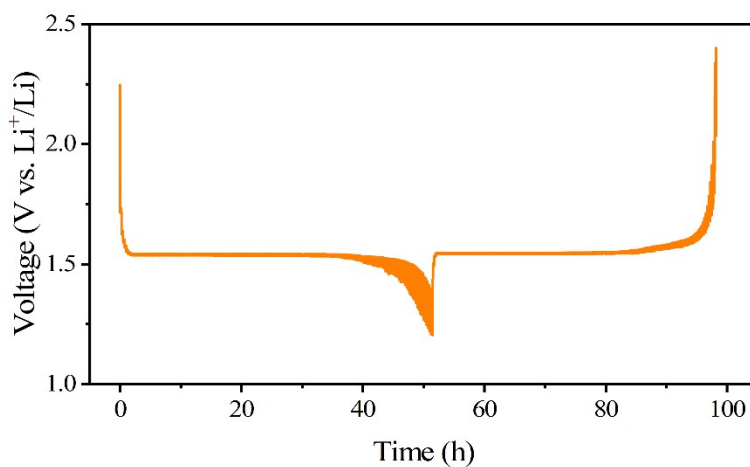


Figure S8. Electrochemical polarization in the GITT test of $\text{Li}_4\text{Ti}_5\text{O}_{12}$.

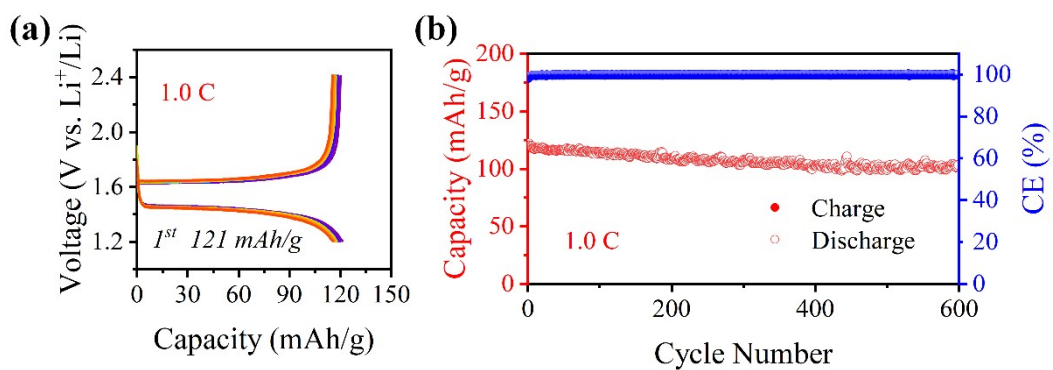


Figure S9. (a) The charge–discharge profile for $\text{Li}_3\text{YCl}_5\text{I}_1$ based $\text{Li-Li}_4\text{Ti}_5\text{O}_{12}$ cells with current densities of 1.0 C and (b) the corresponding cycling performance.

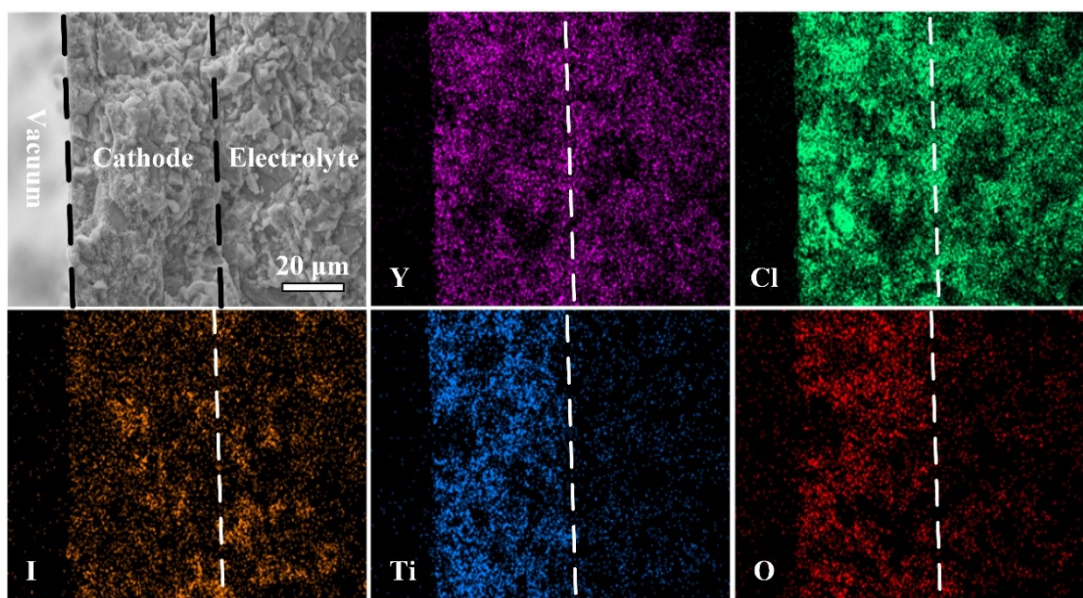


Figure S10. Cross-section SEM image and elemental distributions at the interface between the cathode and electrolyte in $\text{Li-Li}_4\text{Ti}_5\text{O}_{12}$ cell.

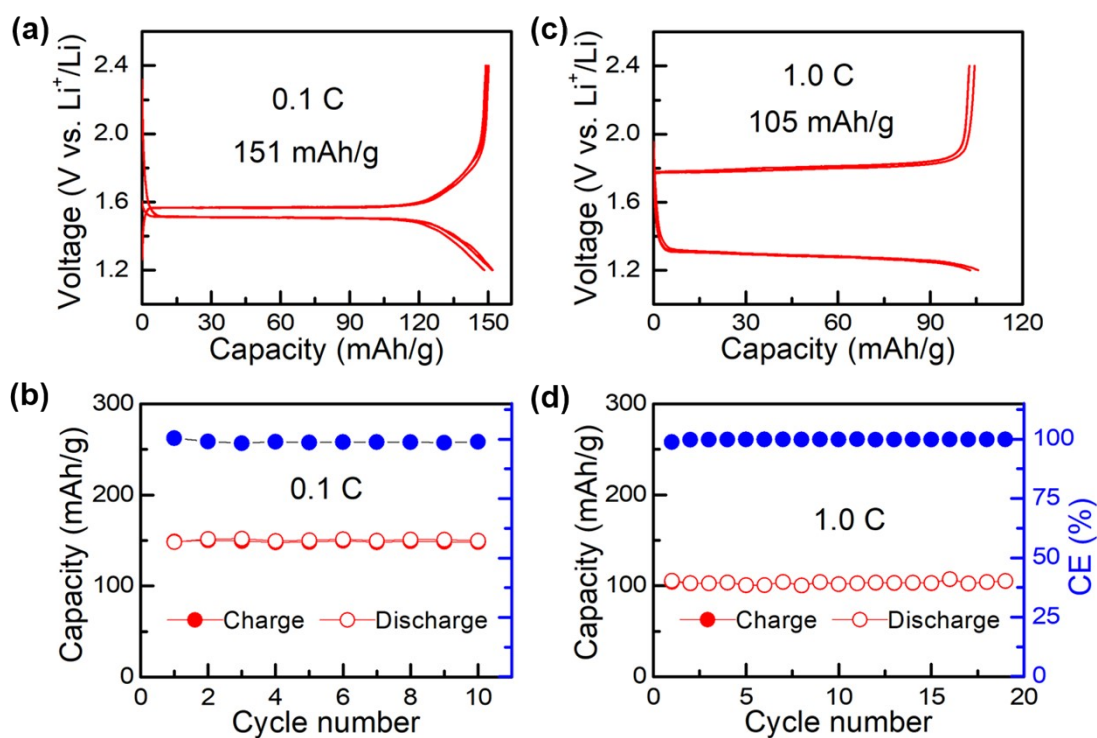


Figure S11. (a, c) The charge–discharge profile for Li_3YCl_6 based $\text{Li-Li}_4\text{Ti}_5\text{O}_{12}$ cells with different current densities (0.1 C, 1.0 C) and (b, d) the corresponding cycling performance.

Table S1. Atomic coordinates of Li_3YCl_6 obtained from XRD Rietveld refinement.

Site	Wyck. Pos.	x	y	z	Occ.
Li1	6h	0.3101(22)	0	0.5	0.5
Li2	6g	0.3310(13)	0	0	1
Y1	2d	1/3	2/3	0.0655(22)	0.03
Y2	2d	1/3	2/3	0.5106(1)	0.97
Y3	1a	0	0	0	1
Cl1	6i	0.2205(2)	0.7794(2)	0.2674(4)	1
Cl2	6i	0.5537(1)	0.4463(1)	0.2448(3)	1
Cl3	6i	0.8856(1)	0.1144(1)	0.2314(4)	1

Table S2. Atomic coordinates of $\text{Li}_3\text{YCl}_5\text{I}_1$ obtained from XRD Rietveld refinement.

Site	Wyck. Pos.	x	y	z	Occ.
Li1	$6h$	0.2910(26)	0	0.5	0.5
Li2	$6g$	0.3420(15)	0	0	1
Y1	$2d$	1/3	2/3	0.0370(40)	0.03
Y2	$2d$	1/3	2/3	0.5098(2)	0.97
Y3	$1a$	0	0	0	1
Cl1	$6i$	0.2212(1)	0.7788(1)	0.2681(4)	0.83
Cl2	$6i$	0.5543(1)	0.4456(1)	0.2447(4)	0.83
Cl3	$6i$	0.8865(1)	0.1135(2)	0.2311(4)	0.83
I1	$6i$	0.2212(1)	0.7788(1)	0.2681(4)	0.17
I2	$6i$	0.5543(1)	0.4456(1)	0.2447(4)	0.17
I3	$6i$	0.8865(1)	0.1135(2)	0.2311(4)	0.17

Table S3. Lattice parameters of $\text{Li}_3\text{YCl}_5\text{I}_1$ and Li_3YCl_6 .

	Li_3YCl_6	$\text{Li}_3\text{YCl}_5\text{I}_1$
Phase	trigonal	trigonal
Space Group	$P\bar{3}m1$	$P\bar{3}m1$
a(Å)	11.2059(2)	11.2615(2)
b(Å)	11.2059(2)	11.2615(2)
c(Å)	6.0401(2)	6.0878(2)
α (°)	90	90
β (°)	90	90
γ (°)	120	120
V(Å ³)	656.85(2)	668.63(3)

Table S4. The Li–X (X = Cl, I) bond lengths in Li₃YCl₅I₁ and Li₃YCl₆ obtained from XRD Rietveld refinement.

Unit : Å	No.	Li ₃ YCl ₆	Li ₃ YCl ₅ I ₁
Li1 (6h) – Cl (6i)	1	2.505(15)	2.399(17)
	2	2.571(3)	2.619(6)
	3	2.505(15)	2.399(17)
	4	2.826(19)	3.010(30)
	5	2.571(3)	2.619(6)
	6	2.826(19)	3.010(30)
Li2 (6g) – Cl (6i)	1	2.526(10)	2.551(12)
	2	2.682(2)	2.707(3)
	3	2.619(11)	2.636(13)
	4	2.619(11)	2.636(13)
	5	2.682(2)	2.707(3)
	6	2.526(10)	2.551(12)

References

- [1] Toby BH. EXPGUI, a graphical user interface for GSAS. *J. Appl. Cryst.* **2001**, *34*, 210-213.
- [2] Momma K, Izumi F. VESTA 3 for three-dimensional visualization of crystal, volumetric and morphology data. *J. Appl. Cryst.* **2011**, *44*, 1272-1276.
- [3] Chen H, Wong LL, Adams S. Softbv - a software tool for screening the materials genome of inorganic fast ion conductors. *Acta. Cryst.* **2019**, *B75*, 18-33.